Article

Electrical Explosion Synthesis, Oxidation and Sintering Behavior of Ti-Al Intermetallide Powders

Marat Lerner [1,2], Alexandr Pervikov [1,2], Elena Glazkova [1,*], Nikolay Rodkevich [1] and Nikita Toropkov [1,2]

[1] Institute of Strength Physics and Material Science, Siberian Branch of Russian Academy of Science, Av. Akademicheskii 2/4, 634055 Tomsk, Russia; lerner@ispms.tsc.ru (M.L.); pervikov@list.ru (A.P.); ngradk@ispms.tsc.ru (N.R.); zerogooff@gmail.com (N.T.)

[2] Research and Education Center Additive Technologies, National Research Tomsk State University, 36 Lenin Ave., 634050 Tomsk, Russia

* Correspondence: eagl@ispms.tsc.ru; Tel.: +7-(3822)-286-938

Abstract: In this research, Ti-Al powders were produced by electrical explosion of twisted titanium and aluminum wires. The resulting powders were pressed and sintered in a vacuum to obtain bulk composites. Transmission electron microscopy (TEM), energy dispersive spectroscopy (EDS), scanning electron microscopy (SEM), and X-ray diffraction (XRD) studies were performed to analyze synthesized powders and bulk composites. The studies carried out showed the presence of α-Ti, α_2-Ti$_3$Al, and γ-TiAl phases, which are formed by coalescence of Ti and Al clusters formed in the process of non-synchronous electrical explosion of twisted wires. Furthermore, an increase in the energy injected into the wires leads to a decrease in the content of micron particles in the powder. During sintering of pressed Ti-Al powder in the range 800–1250 °C, phase transformations occur due to the diffusion of aluminum atoms towards Ti compounds. The research findings can be used to obtain Ti-Al particles and bulk composites with a controllable phase composition.

Keywords: electrical explosion of wires; Ti-Al intermetallic compounds; micro-nano-sized particles; oxidation; sintering

1. Introduction

Intermetallic compounds, especially titanium aluminides, are promising materials for many technical applications due to their attractive properties. These include high-temperature materials for gas turbines, corrosion-resistant materials, and materials for aerospace and automotive engines [1]. Titanium aluminides are characterized by low density, high strength at elevated temperatures, good oxidation and corrosion resistance, etc. [2–4].

Commonly, micron-sized particles of titanium and aluminum are used for the synthesis of Ti-Al-based intermetallics by the sintering of elemental metallic powders. However, the difference in diffusion coefficients between titanium and aluminum is so great that the Kirkendall effect [5,6] occurs where sintering leads to the formation of pores and cracks in the bulk of the material [7,8]. To suppress the formation and growth of the pores and cracks, for example, hot isostatic pressing [8] or spark plasma sintering [9,10] is used, which makes it possible to obtain dense Ti-Al intermetallic compounds. However, pressureless sintering is still a subject of research due to the simplicity and lower cost of the process. For pressureless sintering, it is necessary to suppress the formation and growth of the Kirkendall pores, for example by using synthesized Ti-Al particles.

Thus, Ti-Al intermetallide powders can be obtained by high-energy mechanical milling of a titanium and aluminum elemental powder mixture. Xiao et al. [11] obtained Ti-47% Al (mole fraction) powder by high energy double mechanical milling a mixture of Ti powder (average particle size 150 μm) and Al powder (average particle size 50 μm) under argon. Liu et al. [12] used Ti (size under 0.15 mm) and Al (size under 0.18 mm) powders

to get $Ti_{50}Al_{50}$ (at%) intermetallide. It has been proposed that micron-sized titanium aluminide powders could be obtained by gas atomization of titanium and aluminum melts [10,13]. Mogale et al. [10] demonstrated that the preferred methods to produce titanium aluminide powders are mechanical milling, mechanical alloying, and cryomilling of elemental powders, each of which has its own advantages and disadvantages.

An important disadvantage of γ-TiAl intermetallic compounds is the low plasticity and impact strength at room temperature and low creep resistance at operating temperatures (700–750 °C). Li et al. [14] have shown that a good solution to this problem is the development of fine-grained and nano-structured γ-TiAl materials. Previously, numerous attempts have been made to improve plasticity by refining the grain of alloys to nanoscale [15] or obtaining a fine-grained structure of the intermetallic compound by modifying with boron [16].

A promising way to obtain nanostructured titanium aluminide materials is the consolidation of Ti-Al nanoparticles. Accordingly, it is necessary to develop various methods for the synthesis of Ti-Al intermetallic nanoparticles, which, on the one hand, will avoid the formation of Kirkendall pores, and, on the other hand, will improve the mechanical characteristics of the bulk material. However, as far as we know, methods for the synthesis of γ-TiAl nanoparticles have not been widely studied. Calderon et al. [17] obtained Ti-Al nanoparticles by the mechanical alloying of high purity aluminum and titanium elemental powders (particle sizes less than 200 μm) in a ball mill under an argon atmosphere. Using the spark plasma sintering method of these powders, bulk nano-grained material has been obtained with the chemical compositions of $Al_{41}Ti_{59}$ and average grain size of 137 ± 15 nm. However, methods for producing nanoparticles based on mechanical grinding of elemental powders take a long time, about 700 h. In addition, it is difficult to control the nanoparticle phase composition when grinding and the powders have a wide size distribution. Nanoparticles consisting of TiAl and Ti_3Al phases with an average size of 30 nm were produced by arc melting an Al-Ti ingot in a 50% Ar and 50% H_2 0.1 MPa mixture atmosphere. The disadvantage of this method is a higher generation rate of aluminum vapor compared to that of titanium vapor results in a lower Ti content. Al and Ti atoms in a vapor state collide and grow into Al-Ti clusters. The lower Ti content in vapor can lead to low Ti content in the nanoparticles [18]. Flow-levitation technology was used for the synthesis of nanoparticles consisting of γ-TiAl and $α_2$-Ti_3Al phases with a size of 5–50 nm [14]. The method makes it possible to produce intermetallic compounds of high purity; however, the disadvantage of this technology is its low productivity 3 g/h.

Electrical explosion of wires is a widely used method for producing nanoparticles of metals and metal oxides [19] and has recently been developed to obtain alloy nanoparticles [20,21].

This paper investigates the synthesis method for the preparation of Ti-Al intermetallide particles by the simultaneous electrical explosion of the twisted titanium and aluminum wires and discusses the mechanism of the formation of Ti-Al particles. The sintering behavior of Ti-Al powders and phase evolution when sintering Ti-Al particles is also examined.

2. Materials and Methods

Ti-Al intermetallide particles were obtained by the simultaneous electrical explosion of twisted wires (EETW) of aluminum (0.35 mm in diameter) and titanium (0.32 mm in diameter) on a setup, the schematic diagram of which is shown in Figure 1. The wires are located in a tight container, which is attached to the setup, evacuated, and filled with argon under a pressure of 0.2 MPa. The productivity of the setup is about 200 g/h.
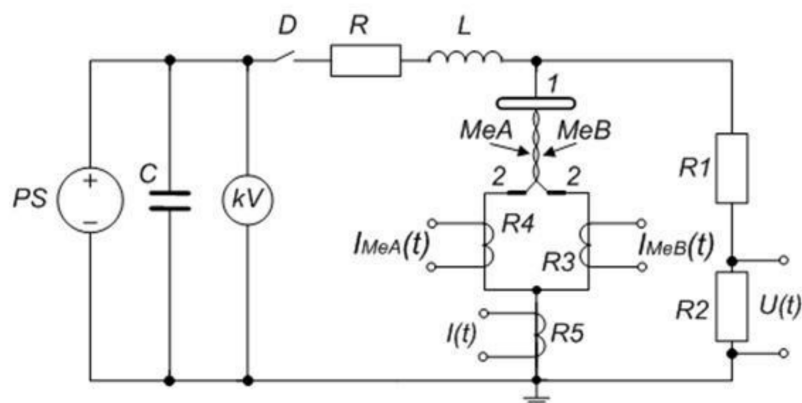
Figure 1. The schematic diagram of the setup for EETW research: R and L–electrical resistance and inductance of the setup: $L = 0.75\ \mu H$, $R = 0.08$ Ohm; capacitor bank capacity $C = 2.8\ \mu F$.

During the experiment, aluminum (*MeA*) and titanium (*MeB*) twisted wires of the length 100 mm (Table 1) are used. The ends of the wires are fixed on a high voltage electrode 1 and two grounded electrodes 2. The high voltage power supply *SP* charges the capacitor bank *C* up to a given voltage *U*, the value of which is monitored by a kilovoltmeter *kV*. On switching the controlled spark gap *D*, the energy stored in *C* is injected into the wires *MeA* and *MeB* and the electrical explosion occurs.

Table 1. Summary of experimental details.

Wire	Wire Diameter, mm	Wire Length, mm	Sublimation Enthalpy, kJ/g	Sublimation Heat $(E_s^{Al}\ i\ E_s^{Ti})$, J
Ti	0.32	100	8.95	326
Al	0.35	100	11	285

The time dependences of voltage $U(t)$ and currents $I(t)$, $I_{MeA}(t)$, and $I_{MeB}(t)$ on the wires were read from the ohmic voltage divider *R1-R2* and Rogowski coils *R3*, *R4*, and *R5* and recorded with a TDS2022B digital oscilloscope. The characteristic times corresponding to different stages of the EETW were determined from the voltage and current oscillograms.

The amount of energy injected into the wires was controlled by the capacitor bank voltage U_0. The determination of the energy amount input into each of the wires *W* was performed based on the time dependences of the current and voltage recorded with the oscilloscope on the current shunt and a voltage divider. Geometrical and energetic parameters of the aluminum and titanium wires used to obtain Ti-Al particles are listed in Table 1. The mass of the wires dispersed approximately corresponded to the ratio of aluminum and titanium in the γ-TiAl intermetallide.

The energy *E* injected into the wires was evaluated from the oscillograms of the discharge current $I(t)$ and voltage $U(t)$ according to Equation (1) [21,22]

$$E = \int_{t_0}^{t_n} U(t)I(t)dt \tag{1}$$

The overheating of the wire metal can be estimated as the E/E_s ratio [19,21], where E_s is the sublimation enthalpy of each of the dispersed metals as presented in Table 1.

The synthesized Ti-Al particles and bulk sintered samples were characterized by transmission electron microscopy (TEM) using a JEM-2100 electron microscope (JEOL, Tokyo, Japan) integrated with an X-Max energy dispersive spectrometer (Oxford Instruments, Abingdon, UK), X-ray diffractometry (XRD) using Shimadzu XRD-7000 diffractometer (Shimadzu, Kyoto, Japan) and scanning electron microscopy (SEM) using LEO EVO 50 electron microscope (Carl Zeiss AG, Jena, Germany) equipped with an INCA-Energy

450 EDS analyzer (Oxford Instruments, Abingdon, UK). The qualitative and quantitative phase composition of the samples (powders and consolidated materials) was estimated using the XPowder software package (XPowder, Granada, Spain) and the database of crystallographic structures PDF2.

The average particle size (a_s) was calculated from the data on the specific surface area (S_s) of the powders according to Equation (2) [19]:

$$a_s = \frac{6}{\rho S_s} \qquad (2)$$

The specific surface area of the powders was determined by the nitrogen adsorption-desorption method using the Sorbtometer M (Katakon, Novosibirsk, Russia) apparatus and calculated by the BET method.

The oxidation behavior of the powders was studied using thermogravimetric analysis (TGA) and differential scanning calorimetry (DSC) apparatus NETZSCH STA 449F3 (Netzsch, Waldkraiburg, Germany). The samples of 5–10 mg were heated in airflow from ambient temperature to 1500 °C at a heating rate of 10 °C min^{-1}.

Bulk composites were obtained by pressing of Ti-Al powder followed by pressureless sintering. For this, a powder sample weighing 1.0 g was pressed in a steel mold under pressure 500 MPa to obtain pellets with a diameter of 10.05 ± 0.05 mm and a thickness of about 5 mm. Cylindrical samples were sintered in a vacuum furnace in the temperature range 800–1250 °C according to the processing scheme shown in Figure 2. The relative density was calculated based on the geometric dimensions of the sintered samples.
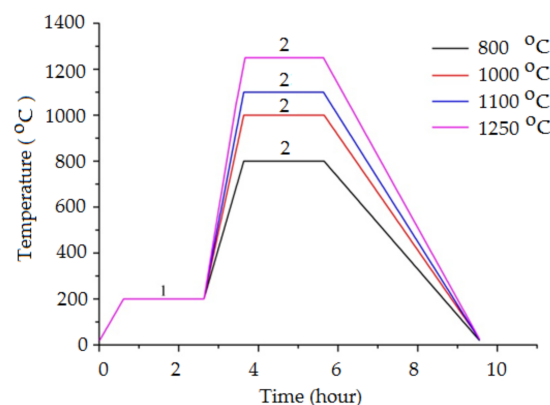

Figure 2. Processing scheme for the sintering of pressed Al-Ti samples.

3. Results and Discussion

3.1. Electrical Explosion Phenomenon

According to the data available in the literature (see, for example, [19]), overheating value E/E_s is one of the main parameters that determine the properties of the nanoparticles synthesized by the electrical explosion of wire. It can be assumed that this parameter will also play a decisive role in the synthesis of the intermetallide particles by the simultaneous electrical explosion of two wires in close contact.

In EETW, the time dependences $I(t)$ and $U(t)$ are crucial for the fundamental understanding of the explosion process. Figure 3 shows the time dependences of the current $I_{Al}(t)$ and the energy injected into the wire $E_{Al}(t)$ for aluminum, the current $I_{Ti}(t)$ and the energy injected $E_{Ti}(t)$ for titanium, total voltage $U(t)$, and current $I(t)$ for twisted wires. The explosion points of Ti and Al wires are designated as $t_{exp}(Ti)$ and $t_{exp}(Al)$, respectively.
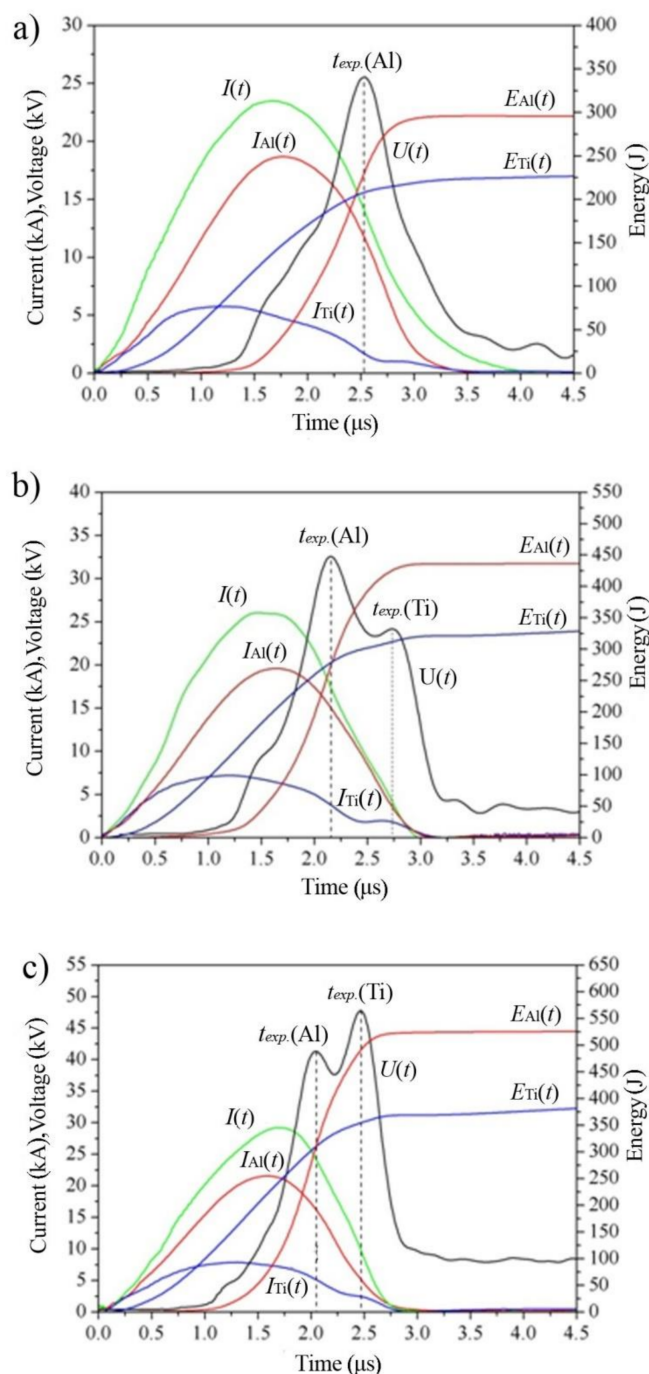
Figure 3. The time dependences of voltage, currents, and energy injected into aluminum and titanium wires for U_0 voltage 22 kV (**a**), 25 kV (**b**), 29 kV (**c**).

As shown in Figure 3, an increase in U_0 from 22 to 29 kV makes it possible to increase the energy $E_{Al}(t)$ injected into the aluminum wire from $1.2E_s$ to $2.1E_s$, and into the titanium wire from $0.82E_s$ to $1.5\ E_s$. At the minimum values of E/E_s when $U_0 = 22$ kV (Figure 3a), there is one local maximum on the $U(t)$ curve, corresponding to the electrical explosion of aluminum wire ($t_{exp} \sim 2.5$ μs). The absence of the second local maximum in the $U(t)$ curve allows us to conclude that titanium wire does not undergo dispersion by electrical explosion due to the low E/E_s value ($E/E_s = 0.82$). Under such conditions, most of the titanium wire is dispersed in the form of liquid metal droplets of micron and submicron sizes [23].

An increase in the energies injected into the wires (Figure 3b,c) leads to an increase in the fraction of energy $E_{Ti}(t)$ injected into the titanium wire and the formation of two sequential local voltage peaks characteristic for the electrical explosion of aluminum and titanium wires [24]. The wires explode sequentially, i.e., non-synchronously. With an increase in E/E_s value, the time interval between wire explosions decreases from 0.67 µs to 0.46 µs.

3.2. Ti-Al Particle Characterization

Figure 4 shows images of the particles prepared by EETW of aluminum and titanium twisted wires at different energy injected levels. It follows from the data presented that with increasing energy injected, a decrease in the average particle size (a_s) calculated from the data on the specific surface area of the powder samples is observed, indicating the increase of the nanoparticle mass fraction. The observed regularity of the decrease in the average size of Ti-Al particles is similar to the typical size of metal particles formed during the electrical explosion of single wires in an inert atmosphere [19]. In addition, with an increase in the energy injected into the wires, a decrease in the number of micron-sized particles is observed in the powders studied.
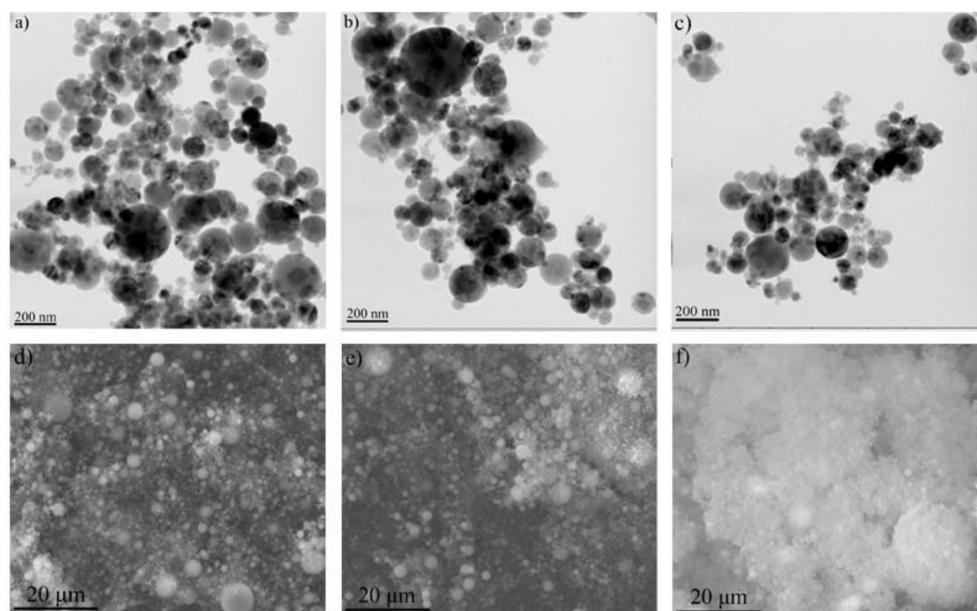

Figure 4. Typical images of Ti-Al particles obtained by simultaneous electrical explosion of titanium and aluminum wires: (**a**,**d**) U_0 = 22 kV, a_s = 240 nm; (**b**,**e**) U_0 = 25 kV, a_s = 178 nm; (**c**,**f**) U_0 = 29 kV, a_s = 133 nm.

The phase composition of the powders obtained at different E/E_s values is mainly represented by the γ-TiAl phase; the powders also contain α-Ti and α_2-Ti$_3$Al (Figure 5). No free aluminum or TiO$_2$ and Al$_2$O$_3$ were found in the powders. According to the Ti-Al phase diagram, the α-Ti phase is a solid solution with an aluminum content of up to 10 at.% [25]. Elemental analysis of Ti-Al particles obtained at various E/E_s values shows that, in general, the particles are equally composed of Ti and Al atoms (Figure 6). An increase in the amount of energy injected into the wires does not lead to a significant change in the phase composition of the powders (Table 2). Only in sample 3, obtained at U_0 = 29 kV, a decrease in the content of the α-Ti phase and an increase in the content of the γ-TiAl phase are observed.
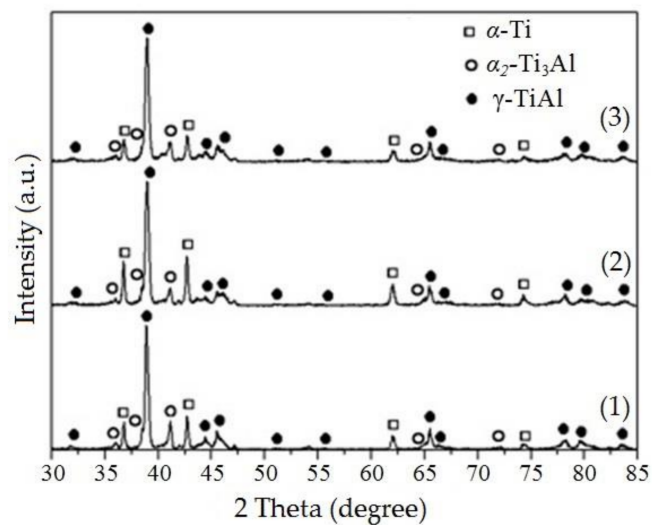
Figure 5. XRD patterns (Cu Kα-radiation) of Ti-Al powders obtained at different energy levels injected into the wires: (1) U_0 = 22 kB; (2) U_0 = 25 kB; (3) U_0 = 29 kB.
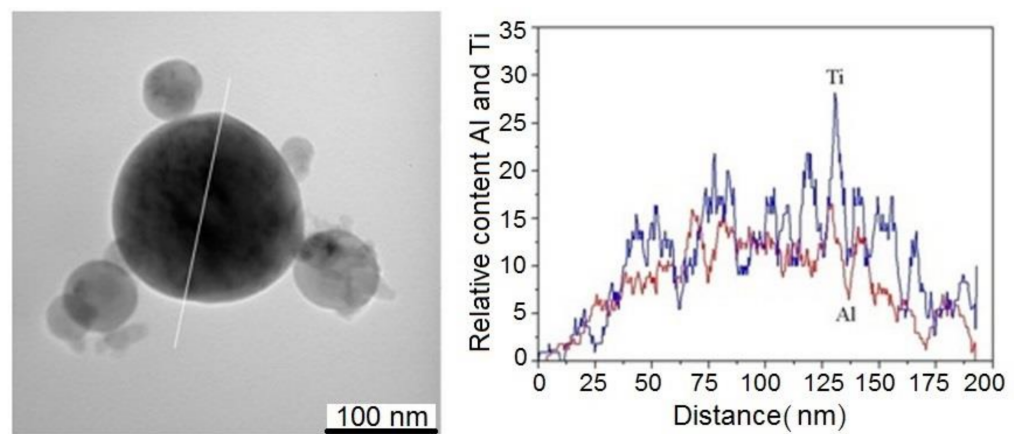

Figure 6. Typical TEM image and line-scan elemental distribution of Ti-Al nanoparticle.

Table 2. The characteristics of Ti-Al powders depending on energy injected into wires.

Sample	U_0, kV	Average Particle Size, nm	Phase Composition, wt.%		
			α-Ti	$α_2$-Ti$_3$Al	γ-TiAl
1	22	240 ± 21	19.4 ± 2.4	8.1 ± 1.1	72.5 ± 7.1
2	25	178 ± 16	22.3 ± 2.7	9.2 ± 1.3	68.3 ± 8.2
3	29	133 ± 13	14.2 ± 1.4	7.8 ± 1.1	78.0 ± 8.7

3.3. Ti-Al Particle Formation

The mechanism of particle formation in the simultaneous electrical explosion of two wires of different metals is determined by the phase state of the explosion products. In the case of the electrical explosion of metals with a high melting point and electrical resistivity (Fe, Ni, Ti, Mo, W), most of the explosion products are in a state of liquid metal droplets of micron and submicron sizes [23]. In the case of the electrical explosion of metals with a low melting point and electrical resistivity (Ag, Cu, Al), the explosion products of wires are represented by a homogeneous mixture of liquid metal clusters and weakly ionized plasma [23,26]. When bimetallic nanoparticles Al-Cu and Al-Ag are obtained using the simultaneous electrical explosion of two wires, homogeneous distribution of the explosion products occurs. Under such conditions, the ratio (in at.%) of metals in a nanoparticle

corresponds to the ratio of metals in wires. The phase composition of the particles formed is in accordance with the phase diagram of binary systems [20,27].

The use of the simultaneous electrical explosion of metal wires with high and low electrical resistivity is accompanied by the formation of explosion products with a complex phase composition. Along with weakly ionized plasma and liquid metal clusters, the explosion products contain liquid droplets of metal with a higher melting point and electrical resistivity. This leads to the formation of particles in a state of binary melt with different metal ratios in the explosion products: nano-sized particles with a metal ratio close to that in the wire and micron/submicron particles with a higher content of metal with high electrical resistivity. This feature of the phase state of the metal explosion products with high and low electrical resistivity leads to the formation of a more complex composition phase of particles that does not correspond to the phase diagram of binary systems. These regularities of the phase formation were observed in the Ni-Al samples in [28,29].

The EETW products of titanium and aluminum wires contain micron and submicron titanium particles. Upon coalescence of the explosion products of titanium and aluminum wires, micron titanium particles will be alloyed with aluminum, which creates conditions for the formation of α-Ti and α_2-Ti$_3$Al phases. The ratio of metals in nano-sized particles formed is close to that of metals in wires, which creates conditions for the formation of nanoparticles with a γ-TiAl structure. An increase in the energy injected into the wires in the investigated range $U_0 = 22$–29 kV leads to a decrease in the number and size of micron titanium droplets, as a result, the content of α-Ti and α_2-Ti$_3$Al phases in the EETW products decreases. A decrease in the content of micron titanium particles can also be achieved by additional heating of the expanding EEW products at the stage of the arc [30]. SEM/EDX elemental map revealed the formation of Ti-Al particles with the homogeneous dispersion of Ti and Al atoms within the particles as shown in Figure 7 as well as the formation of both titanium and aluminum particles.
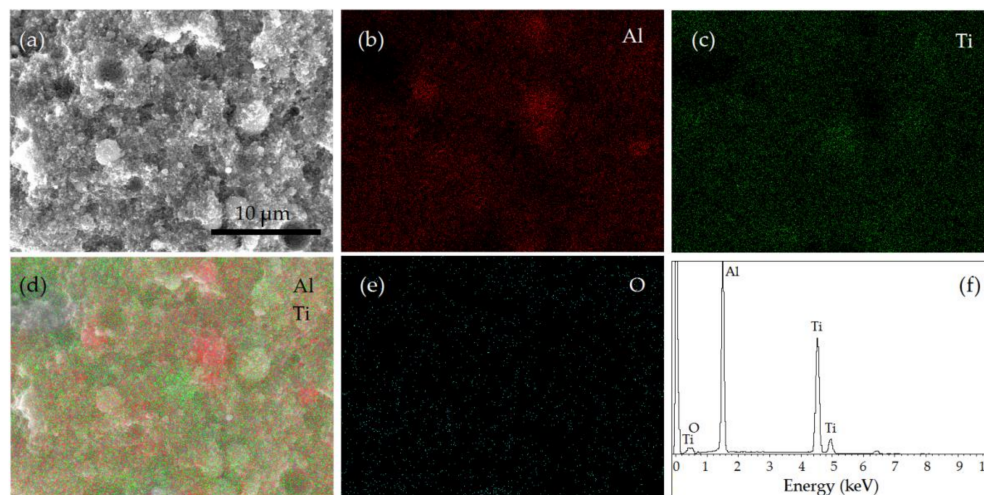

Figure 7. SEM image (**a**) and SEM/EDX analysis (**b–f**) of Ti-Al powder obtained at $U_0 = 29$ kV.

3.4. Ti-Al Particle Oxidation

The oxidation process of metal powders is a series of sequential stages. The oxidation process is controlled by the diffusion of reactive species through the oxide layer on the surface of the nanoparticles. The transition of the oxidation process to the next stage is due to the recrystallization of the surface oxide phases when the integrity of the oxide layer is disrupted [31,32].

Thermogravimetry is a very versatile technique for studying the oxidation behavior of metallic powders. For the study, the Ti-Al nanopowders with an average particle size of 133 nm were used, the nanoparticles were obtained at $U_0 = 29$ kV. The TGA-DSC curves of the Ti-Al nanopowder are shown in Figure 8. When the nanopowder heating

in the temperature range from ambient temperature to ≈290 °C, a negligible change in the sample mass is observed, probably due to the desorption of ambient gases from the surface. Starting from a temperature of 290 °C, the oxidation of nanoparticles is observed, accompanied by continuous heat release, the intensity of which increases with increasing temperature and by an increase in the sample mass.
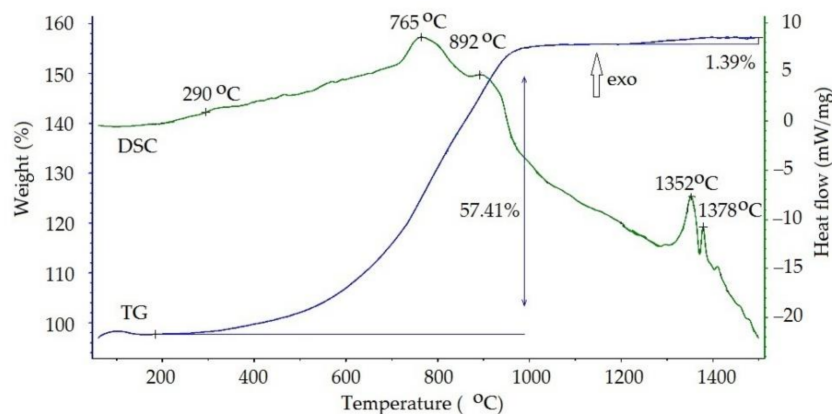

Figure 8. DSC and TG curves of Ti-Al particles.

Above 700 °C, the oxidation rate increases significantly, which follows from a sharp increase in the sample mass and the heat release rate. The maximum oxidation rate is reached at a temperature of about 765 °C. Reaching 1000 °C the oxidation rate is minimal. This temperature is the point of completion of the rapid nanopowder oxidation. Then the next stage of nanopowder oxidation begins, characterized by a second exothermic peak with a maximum at 1352–1378 °C.

The oxidation process is a series of sequential stages and the oxidation process in s single stage can, thus, be assumed to be a simple chemical heterogeneous reaction. The dependence of the conversion degree of the heterogeneous solid-gas reaction on time and accordingly on temperature under the conditions of thermal analysis has an S-shaped character.

Thus, the curve can be divided into a series of S-shaped curves, each of which characterizes the oxidation process at the corresponding stage.

Analyzing the thermogravimetric data [33,34] can describe the sample mass change during the oxidation process by the approximate Equation (3)

$$M(T) = M_0 + \sum_{i=1}^{N} M_i \alpha_i(T) \tag{3}$$

where N number of process stages; M_0 mass of nanopowder sample; M_i sample mass gain at i-th stage; α_i—conversion degree; T—absolute temperature.

Conversion degree as a function of temperature can be represented as (4)

$$\alpha = \frac{1}{1 + \exp\left[\frac{-2\pi(T-T_0)}{\Delta T}\right]} \tag{4}$$

depending on two parameters: characteristic temperature T_0, the temperature of maximum reaction rate, and reaction temperature range ΔT where the approximately 90% conversion takes place.

As follows from the given curves, good agreement of the data is observed. The calculated parameters are shown in Table 3. Based on the parameter values calculated, the reaction temperature ranges are deduced.

Table 3. Calculated parameters of the Ti-Al powder oxidation process.

Stage	Mass Gain, %	T_0, °C	Range, °C	ΔT, °C
I	19,3	614	326–903	576
II	26,8	780	634–925	290
III	12,2	903	824–983	159
IV	1,5	1288	1159–1417	257

As follows from the data presented the oxidation of Ti-Al powder is a sequence of 4 stages proceeding sequentially. The oxidation reaction at stage I proceeds due to the diffusion of the oxygen through the native oxide layer which determines its low rate. The oxidation reaction at stage II is characterized by a higher rate due to the amorphous oxide-anatase phase transition, while stage III is due to the anatase-rutile phase transition. Most of the powder is oxidized below a temperature of 1000 °C, the contribution of the oxidation process occurring at temperatures above 1000 °C is negligible.

3.5. Characterization of the Sintered Ti-Al Structures

To prevent oxidation of the Ti-Al powders, the sintering of the samples was carried out in a vacuum. To study the sintering behavior of Al-Ti powders in the temperature range 800–1250 °C, the pellets were prepared from the powder obtained at the maximum energy injected into the wires (U_0 = 29 kV), and the particles had a minimum average size (a_s = 133 nm), and the content of γ-TiAl was 78 wt%. The pellets prepared had an average relative density of 0.57 of the theoretical (TD). The pellets were sintered according to the processing scheme shown in Figure 2. The scheme suggests two processing stages. Stage 1 is a degasification process when the removal of adsorbed gases from the particle surface takes place. At stage 2 the particles are directly sintered.

Figure 9 shows the fracture surfaces demonstrating the microstructural evolution of the samples sintered according to the processing scheme at a temperature ranging from 800 to 1250 °C as shown in Figure 2. Figure 9a shows an SEM image of the pristine Al-Ti powder. The data presented reveal that the powder consists of spherical nano- and microparticles. Nanoparticles partly located at the surface of the microparticles are partly aggregated and located among the microparticles forming randomly assembled 3D structures.

Exposure of the sample to 800 °C results in the formation of a continuous network (Figure 9b). Nanoparticles located at the surface of the microparticles are fully fused. The nanoparticle aggregates located in the interparticle space are fused among themselves. The spherical structure of both of the nanoparticles and the microparticles is somewhat conserved. The sample density increases to 0.65 TD. Sintering at 1000 °C, shows deeper transformation (Figure 9c). Particles are mostly fused and the initial particle microstructure is not observable. The polyhedron structure is quite pronounced and the original shape of the particles is not discerned. The density of the sample increases to 0.8 TD. Figure 9d (1250 °C) shows clearly that the sample is actually sintered completely. Microstructure formed is presented with polyhedron-shaped grains but not spherical particles. The particulate structure of the sample disappears, forming a lamellar structure that is well-known [35]. Porosity is still noticeable though the pores are small and rounded with the sample relative density being 0.92 TD.

Figure 10 shows the XRD spectra of the samples sintered according to the processing scheme shown in Figure 2. The quantitative phase composition of the sintered samples is presented in Table 4. The XRD pattern shows that the sample sintered at 800 °C contains γ-TiAl and TiO phases. The presence of the TiO phase is assumed to be a result of the oxidation of the α-Ti phase. The presence of titanium oxide in the sintered sample indicates that the incomplete degassing of the pressed powder occurring as a result of which oxygen at high temperatures diffuses into the titanium lattice to form the TiO phase. However, it is difficult to eliminate the oxygen during the fabrication of Ti powders. Additionally, the existence of a small amount of oxygen results in a strengthening of Ti alloys [36,37].
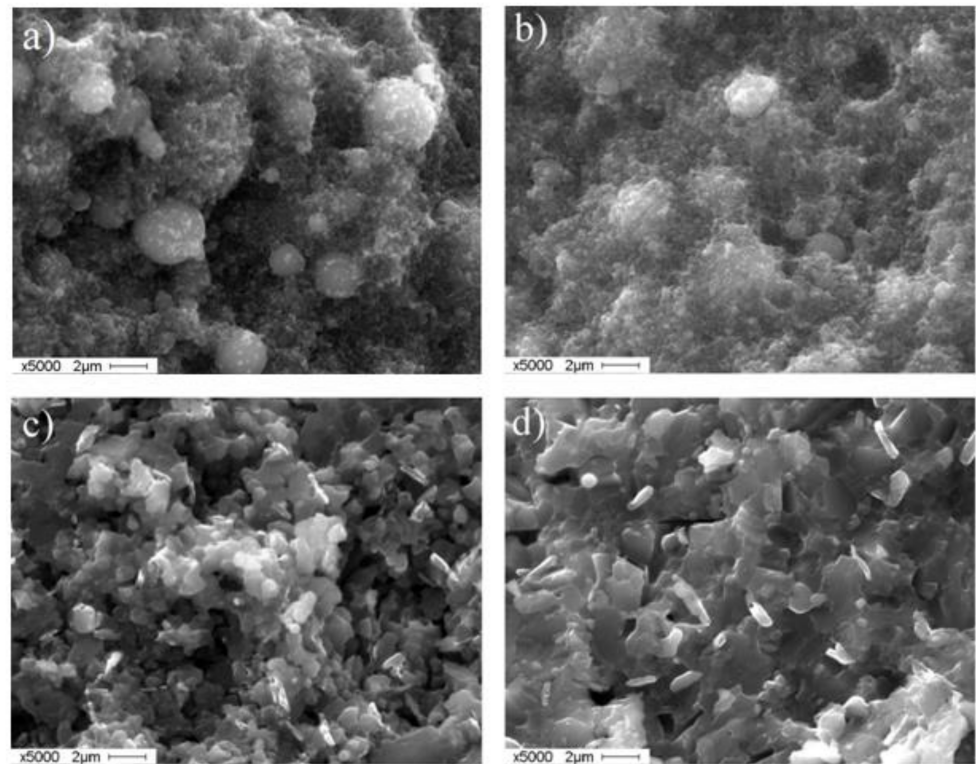
Figure 9. Fracture surfaces of specimens sintered at different temperatures: (**a**) 25 °C, (**b**) 800 °C, (**c**) 1000 °C, (**d**) 1250 °C.
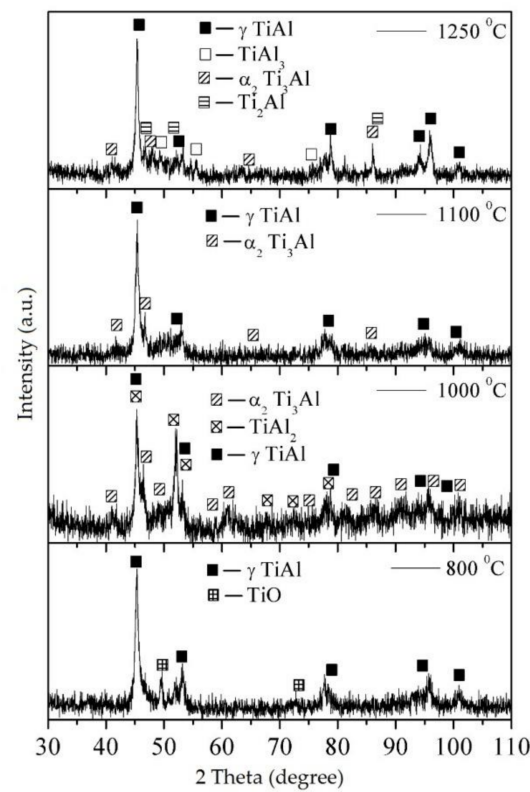

Figure 10. X-ray data for sintering of Ti-Al samples (Co Kα-radiation).

Table 4. Phase composition of sintered Ti-Al samples.

Sintering Temperature, °C	Phase Composition, wt.%					
	TiO	Ti$_2$Al	α_2-Ti$_3$Al	γ-TiAl	TiAl$_2$	TiAl$_3$
800	17.3 ± 1.5	—	—	82.7 ± 8.1	—	—
1000	—	—	15.5 ± 1.2	42.4 ± 4.3	42.1 ± 4.3	—
1100	—	—	12.4 ± 1.0	87.6 ± 8.6	—	—
1250	—	12.1 ± 1.1	25.6 ± 2.3	47.0 ± 5.5	—	15.3 ± 1.3

Sintering the pressed sample at a temperature of 1000 °C leads to a change in the phase composition. This change can be caused by the intensification of diffusion processes when increasing sintering temperature. The lack of titanium oxide XRD peaks suggests that the oxide layer on the surface of micron titanium particles is either absent or is in an X-ray amorphous state. This creates conditions for the diffusion of aluminum in areas depleted in aluminum, which leads to the implementation of the phase transformation α-Ti $\rightarrow \alpha_2$-Ti$_3$Al. The samples having been calcined at 1000 °C, Ti, and Al distribution characteristics are maintained the same as in pristine powder (Figure 11). A further increase in the sintering temperature of the samples to 1100 and 1250 °C does not lead to a significant change in the phase composition of the sample. The formation of the TiAl$_3$ and TiAl$_2$ phases is most likely the result of diffusion processes in the material. The presence of structural defects in the form of grain boundaries, microcracks, micropores prevents the diffusion of aluminum in the bulk of the material, which leads to the formation of phases enriched with aluminum [38–40].
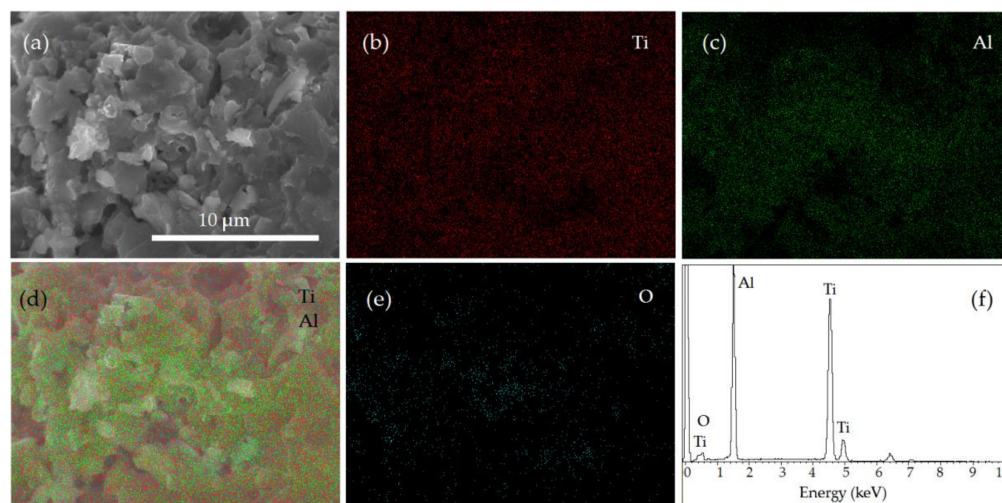
Figure 11. SEM image (**a**) and SEM/EDX analysis (**b**–**f**) of Ti-Al sample sintered at 1000 °C.

4. Conclusions

The simultaneous electrical explosion of the aluminum and titanium twisted wires leads to the formation of micron, submicron, and nano-sized Ti-Al particles. An increase in the energy injected into the wires at EETW leads to a decrease in the fraction of micron-sized Ti-Al particles, with the average Ti-Al particle size decreasing from 240 to 133 nm. A likely mechanism for the formation of Ti-Al particles is the coalescence and coagulation of Ti and Al clusters with the formation of the α-Ti, α_2-Ti$_3$Al, and γ-TiAl phases. The ratio of the phases is determined by the titanium and aluminum diffusion and phase formation rates depending on the cluster sizes.

Ti-Al intermetallic powder is easily oxidized in air, and most of it is oxidized to a temperature of 1000 °C. Therefore, the sintering of pressed samples should be carried out in a vacuum furnace. When sintering pressed samples of Ti-Al particles in the temperature range 800–1250 °C, the Ti$_2$Al, TiAl$_2$, and TiAl$_3$ phases are formed due to the diffusion of

Al towards Ti as a result of the higher diffusion coefficient of aluminum compared to that of titanium.

The simultaneous electrical explosion of the twisted metal wires is a productive, versatile, and adaptable method when producing intermetallic compounds suitable for powder metallurgy applications. From the data obtained, it can be concluded that the simultaneous electrical explosion of the aluminum and titanium twisted wires can be used to obtain Ti-Al powder, which is promising for the production of bulk composites.

Author Contributions: Conceptualization, M.L., E.G. and N.R.; methodology, M.L. and E.G.; validation, N.R. and A.P.; investigation, A.P. and N.T.; data curation, N.R., A.P. and N.T.; writing original draft preparation, M.L., E.G. and N.R.; review and editing, E.G. and N.R.; supervision, M.L. and E.G.; project administration, M.L.; funding acquisition, M.L. All authors have read and agreed to the published version of the manuscript.

Conflicts of Interest: The authors declare no conflict of interest.

References

1. Cinca, N.; Lima, C.R.C.; Guilemany, J.M. An overview of intermetallics research and application: Status of thermal spray coatings. *J. Mater. Res. Technol.* **2013**, *2*, 75–86. [CrossRef]
2. Brotzu, A.; Felli, F.; Marra, F.; Pilone, D.; Pulci, G. Mechanical properties of a TiAl-based alloy at room and high temperatures. *Mater. Sci. Technol.* **2018**, *34*, 1847–1853. [CrossRef]
3. Clemens, H.; Mayer, S. Intermetallic titanium aluminides in aerospace applications–processing, microstructure and properties. *Mater. High Temp.* **2016**, *33*, 560–570. [CrossRef]
4. Bewlay, B.P.; Nag, S.; Suzuki, A.; Weimer, M.J. TiAl alloys in commercial aircraft engines. *Mater. High Temp.* **2016**, *33*, 549–559. [CrossRef]
5. Wang, G.-X.; Dahms, M. Synthesizing gamma-TiAl alloys by reactive powder processing. *JOM* **1993**, *45*, 52–56. [CrossRef]
6. Lee-Sullivan, P. HIP processing of Ti-Al intermetallic using blended elemental powder. *J. Mater. Process. Technol.* **1993**, *38*, 1–13. [CrossRef]
7. Wang, G.-X.; Dahms, M. An effective method for reducing porosity in the titanium aluminide alloy $Ti_{52}Al_{48}$ prepared by elemental powder metallurgy. *Scr. Metall. Mater.* **1992**, *26*, 1469–1474. [CrossRef]
8. Dahms, M.; Schmelzer, F.; Seeger, J.; Wildhagen, B. Microstructure and Mechanical Properties of γ Base Titanium Aluminide Produced from Extruded Elemental Powders. *Mater. Sci. Technol.* **1992**, *8*, 359–362. [CrossRef]
9. Kennedy, S.; Rao, S.K.T.S. Densification of γ-TiAl Powders by Spark Plasma Sintering. *Mater. Sci. Forum* **2012**, *710*, 303–307. [CrossRef]
10. Mogale, N.F.; Matizamhuka, W.R. Spark Plasma Sintering of Titanium Aluminides: A Progress Review on Processing, Structure-Property Relations, Alloy Development and Challenges. *Metals* **2020**, *10*, 1080. [CrossRef]
11. Xiao, S.; Tian, J.; Xu, L.; Chen, Y.; Yu, H.; Han, J. Microstructures and mechanical properties of TiAl alloy prepared by spark plasma sintering. *Trans. Nonferrous Met. Soc. China* **2009**, *19*, 1423–1427. [CrossRef]
12. Liu, Y.; Liu, W. Mechanical alloying and spark plasma sintering of the intermetallic compound Ti50Al50. *J. Alloys Compd.* **2007**, *440*, 154–157. [CrossRef]
13. Gerling, R.; Clemens, H.; Schimansky, F.P. Powder metallurgical processing of intermetallic gamma titanium aluminides. *Adv. Eng. Mater.* **2004**, *6*, 23–38. [CrossRef]
14. Li, X.B.; Zhang, J.B.; Ji, X.C.; Wu, X.Q.; Luo, J.S.; Tang, Y.J. A Small Patch Production of γ-TiAl Alloys Nanoparticles via Physical Vapor-phase Method. *Integr. Ferroelectr.* **2013**, *147*, 146–153. [CrossRef]
15. Froes, F.H.; Senkov, O.N.; Baburaj, E.G. Synthesis of nanocrystalline materials. *Mater. Sci. Eng. A* **2001**, *301*, 44–53. [CrossRef]
16. Wu, X. Review of alloy and process development of TiAl alloys. *Intermetallics* **2006**, *14*, 1114–1122. [CrossRef]
17. Calderon, H.A.; Garibay-Febles, V.; Umemoto, M.; Yamaguchi, M. Mechanical properties of nanocrystalline Ti–Al–X alloys. *Mater. Sci. Eng. A* **2002**, *329–331*, 196–205. [CrossRef]
18. Liu, T.; Zhang, T.; Zhu, M.; Qin, C. Synthesis and structures of Al–Ti nanoparticles by hydrogen plasma-metal reaction. *J. Nanopart. Res.* **2012**, *14*, 738. [CrossRef]
19. Kotov, Y.A. Electric Explosion of Wires as a Method for Preparation of Nanopowders. *J. Nanopart. Res.* **2003**, *5*, 539–550. [CrossRef]
20. Pervikov, A.V.; Kazantsev, S.O.; Lozhkomoev, A.S.; Lerner, M.I. Bimetallic Al/Ag, Al/Cu and Al/Zn nanoparticles with controllable phase compositions prepared by the electrical explosion of two wires. *Powder Technol.* **2020**, *372*, 136–147. [CrossRef]
21. Pervikov, A.V.; Suliz, K.V.; Lerner, M.I. Nanoalloying of clusters of immiscible metals and the formation of bimetallic nanoparticles in the conditions of non-synchronous explosion of two wires. *Powder Technol.* **2020**, *360*, 855–862. [CrossRef]

22. Lerner, M.I.; Pervikov, A.V.; Glazkova, E.A.; Svarovskaya, N.V.; Lozhkomoev, A.S.; Psakhie, S.G. Structures of binary metallic nanoparticles produced by electrical explosion of two wires from immiscible elements. *Powder Technol.* **2016**, *288*, 371–378. [CrossRef]

23. Sarkisov, G.S.; Sasorov, P.V.; Struve, K.W.; McDaniel, D.H. State of the metal core in nanosecond exploding wires and related phenomena. *J. Appl. Phys.* **2004**, *96*, 1674–1686. [CrossRef]

24. Pervikov, A.; Glazkova, E.; Lerner, M. Energy characteristics of the electrical explosion of two intertwined wires made of dissimilar metals. *Phys. Plasmas* **2018**, *25*, 070701. [CrossRef]

25. Kattner, U.R.; Lin, J.C.; Chang, Y.A. Thermodynamic Assessment and Calculation of the Ti-Al system. *Metall. Trans. A* **1992**, *23*, 2081–2090. [CrossRef]

26. Romanova, V.M.; Ivanenkov, G.V.; Mingaleev, A.R.; Ter-Oganesyan, A.E.; Tilikin, I.N.; Shelkovenko, T.A.; Pikuz, S.A. On the phase state of thin silver wire cores during a fast electric explosion. *Phys. Plasmas* **2018**, *25*, 112704. [CrossRef]

27. Pervikov, A.; Lerner, M. Mechanism of the formation of the structure and phase state of binary metallic nanoparticles obtained by the electric explosion of two wires made of different metals. *Curr. Appl. Phys.* **2017**, *17*, 1494–1500. [CrossRef]

28. Ishihara, S.; Koishi, T.; Orikawa, T.; Suematsu, H.; Nakayama, T.; Suzuki, T.; Niihara, K. Synthesis of intermetallic NiAl compound nanoparticles by pulsed wire discharge of twisted Ni and Al wires. *Intermetallics* **2012**, *23*, 134–142. [CrossRef]

29. Abraham, A.; Nie, H.; Schoenitz, M.; Vorozhtsov, A.; Lerner, M.; Pervikov, A.; Rodkevich, N.; Dreizin, E. Bimetal Al–Ni nano-powders for energetic formulations. *Combust. Flame* **2016**, *173*, 179–186. [CrossRef]

30. Bora, B.; Kausik, S.S.; Wong, C.S.; Chin, O.H.; Yap, S.L.; Soto, L. Observation of the partial reheating of the metallic vapor during the wire explosion process for nanoparticle synthesis. *Appl. Phys. Lett.* **2014**, *104*, 223108. [CrossRef]

31. Vorozhtsov, A.B.; Lerner, M.; Rodkevich, N.; Nie, H.; Abraham, A.; Schoenitz, M.; Dreizin, E.L. Oxidation of nano-sized aluminum powders. *Thermochim. Acta* **2016**, *636*, 48–56. [CrossRef]

32. Ouyang, P.; Mi, G.; Li, P.; He, L.; Cao, J.; Huang, X. Non-Isothermal Oxidation Behaviors and Mechanisms of Ti-Al Intermetallic Compounds. *Materials* **2019**, *12*, 2114. [CrossRef]

33. Vorozhtsov, A.B.; Rodkevich, N.G.; Bondarchuk, I.S.; Lerner, M.I.; Zhukov, A.S.; Glazkova, E.A.; Bondarchuk, S.S. Thermokinetic investigation of the aluminum nanoparticles oxidation. *Int. J. Energetic Mater. Chem. Propuls.* **2017**, *16*, 309–320. [CrossRef]

34. Bondarchuk, I.S.; Bondarchuk, S.S.; Borisov, B.V. Identification of kinetic triplets by results of derivatographic analysis. *MATEC Web Conf.* **2018**, *194*, 01010. [CrossRef]

35. Jones, S.A.; Kaufman, M.J. Phase equlibria and transformations in intermediate titanium–aluminum alloys. *Acta Metall. Mater.* **1993**, *41*, 387–398. [CrossRef]

36. Bahador, A.; Umeda, J.; Yamanoglu, R.; Bakar, T.A.A.; Kondoh, K. Strengthening evaluation and high-temperature behavior of Ti–Fe–O–Cu–Si alloy. *Mater. Sci. Eng. A* **2021**, *800*, 140324. [CrossRef]

37. Bahador, A.; Umeda, J.; Ghandvar, H.; Bakar, T.A.A.; Yamanoglu, R.; Issariyapat, A.; Kondoh, K. Microstructure globularization of high oxygen concentration dual-phase extruded Ti alloys via powder metallurgy route. *Mater. Charact.* **2021**, *172*, 110855. [CrossRef]

38. Wan, Q.; Li, F.; Wang, W.; Hou, J.; Cui, W.; Li, Y. Study on In-Situ Synthesis Process of Ti–Al Intermetallic Compound-Reinforced Al Matrix Composites. *Materials* **2019**, *12*, 1967. [CrossRef]

39. Thiyaneshwaran, N.; Sivaprasad, K.; Ravisankar, B. Nucleation and growth of TiAl$_3$ intermetallic phase in diffusion bonded Ti/Al Metal Intermetallic Laminate. *Sci. Rep.* **2018**, *8*, 16797. [CrossRef]

40. Xu, L.; Cui, Y.Y.; Hao, Y.L.; Yang, R. Growth of intermetallic layer in multi-laminated Ti/Al difusion couples. *Mater. Sci. Eng. A* **2006**, *435–436*, 638–647. [CrossRef]